NOn-transferred MAgnetization Ratio (NOMAR) Filtering: A New Technique to Create Tissue Selective CEST contrast maps

Guanshu Liu[1,2], Kannie WY Chan[2,3], Xiaolei Song[2,3], Jiangyang Zhang[2,4], Assaf A Gilad[2,3], Jeff WM Bulte[2,3], Peter CM van Zijl[2,4], and Michael T McMahon[2,4]

[1]F.M. Kirby Research Center for Functional Brain Imaging, Kennedy Krieger Instittute, Baltimore, Maryland, United States, [2]Department of Radiology, Johns Hopkins University School of Medicine, baltimore, maryland, United States, [3]Cellular Imaging Section, Institute for Cell Engineering, Johns Hopkins University School of Medicine, baltimore, maryland, United States, [4]F.M. Kirby Research Center for Functional Brain Imaging, Kennedy Krieger Institute, baltimore, maryland, United States

INTRODUCTION

Recently, Chemical Exchange Saturation Transfer (CEST) has emerged as a promising MRI contrast mechanism[1,2]. One of the desirable features of CEST contrast is its inherent quantitative capability. However, when applied *in vivo*, properties such as water and macromolecular concentrations in the tissue containing a CEST agent must be taken into consideration. For instance, the presence of fat or endogenous CEST contrast (e.g., from, urea in the bladder[3], endogenous peptides and proteins in tumors[4], or glycogen in liver[5]) may produce noticeable frequency dependent contrast in the MTR_{asym} maps used to quantify CEST. To overcome this challenge, we propose a magnetization transfer (MT) based segmentation technique for globally filtering CEST contrast maps. MT contrast was chosen because it is known to allow tissue classification,[6,7] for example the separation of CSF containing pixels from brain parenchyma in MS studies[8] and removal of background tissue from contrast-enhanced blood signal[9]. Here, we demonstrate how this simple MT segmentation technique can be applied to improve *in vivo* detection of DIACEST Liposome (DL) contrast.

METHODS AND MATERIALS

Phantom and *in vitro* MRI: A phantom was prepared consisting of either 0 or 10 mM L-arginine (Larg, Sigma) and 0%, 5%, 10%, 15%, or 20% heat-cross-linked (80°C, 10 minutes) Bovine Serum albumin (BSA, Sigma) in 0.01 M PBS (pH=7.3)[10], and imaged on a 9.4T Bruker scanner using the *in vitro* CEST MRI acquisition described previously[13]. We acquired MT-weighted (MT-w) images ($\omega_1/2\pi$=150 Hz, t_{sat}=3 sec) with the saturation frequency swept from -100 ppm (-40 kHz) to 100 ppm (40 kHz) in 5 ppm (2 kHz) steps. An unsaturated image (S_0) was also acquired with the same t_{sat} but $\omega_1/2\pi$=0.

In vivo MRI: Eight-week old C57BL/6.SJL mice bearing the CD45.1 alloantigen (Jackson Labs) were injected with a cancer cell vaccine (irradiated B16 melanoma and B78-H1 GM-CSF-expressing bystander melanoma cells)[12] to produce an immunoresponsive enlargement of the popliteal lymph nodes 1 week prior to DL injection. Fresh Larg DLs (~ 100 nm) were prepared as described previously[11], and intradermally injected (40 µL, ~30 nM DL solutions) into the right hind footpad of mice. *In vivo* CEST-MRI was conducted on a horizontal 9.4T Bruker scanner 24 hours after injection using the method described previously[11]. The MT-w images were acquired at -12.5 ppm and -50 ppm using $\omega_1/2\pi$=150Hz, t_{sat}=3 sec.

Post-processing: All data were processed using custom-written Matlab scripts. The CEST contrast was quantified by calculating MTR_{asym}[11]. ROI masks were drawn manually based on the $T2_w$-images. NOrmalized MAgnetization Ratio (NOMAR) filtering was conducted using the following procedure. First, a NOMAR map was generated using the MT-w images with saturation offsets of -12.5 ppm and -50 ppm, i.e. *NOMAR=S(-12.5 ppm)/S(-50 ppm)*. Next, a pixel count vs NOMAR histogram was generated and fit to a mixed Gaussian distribution using the expectation-maximation (EM) algorithm in the Matlab function 'fit_mix_gaussian.m'. For *in vitro* images, we performed one signal Gaussian fitting for each ROI, and for the *in vivo* images, we assumed three independent Gaussian functions (three compartments: low, moderate, and high water content) to fit all pixels of the image. The threshold for tissue segmentation was initially determined by finding the point in the histogram where the high water content compartment crossed the moderate water content compartment for one mouse and kept between 0.70-0.75 for all mice. All pixels possessing a higher ratio than this were removed from the subsequent images.

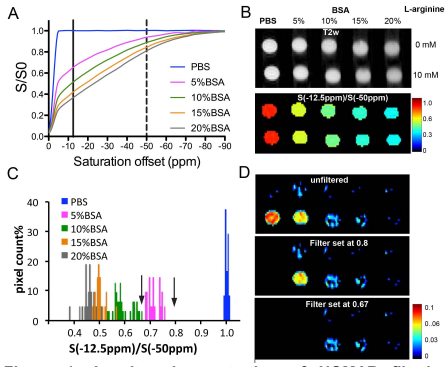

Figure 1. *In vitro* demonstration of NOMAR filtering of samples containing different concentrations of cross-linked BSA. A) frequency dependency of MT contrast for the cross-linked BSA samples; **B**) T2-w image (top) and NOMAR map (bottom) of samples containing 0%-20% cross-linked BSA with or without 10 mM Larg; **C**) NOMAR histogram, with arrows pointing to 0.80 and 0.67 thresholds; D) MTR_{asym} maps before (top) and after NOMAR filtering with the threshold set to 0.80 (middle) or 0.67 (bottom).

RESULTS AND DISCUSSION

Based on the previous studies[7] and our simulations, we proposed to use MT-w images at -12.5 ppm to separate tissues where CEST agent may localize. To reduce the possible influence of B1 inhomogeneity, we normalized S(-12.5 ppm) with a reference image, S(-50 ppm), to produce a new metric, NOMAR. To prove this NOMAR value can effectively separate tissues with different semi-solid concentrations, we first tested it on a phantom containing tubes either with or without the CEST contrast agent (10 mM Larg) embedded in cross-linked BSA (0-20%). As shown in Figs. 1A&1B, the NOMAR value strongly correlated with the BSA (or water) concentration, varying from 1.00 to 0.37 as BSA concentration increased from 0 to 20%. With the histogram shown in Fig. 1C, we could determine the threshold to separate samples by the concentration of BSA. As shown in Fig 1D, compartment-selective CEST contrast maps were produced by applying NOMAR filters at 0.80 or 0.67 to remove pixels containing the lowest concentrations of BSA (i.e. 0% and 5% BSA respectively). The presence of CEST agents did not significantly alter the segmentation. By filtering with an appropriate NOMAR threshold, the CEST contrast in samples containing higher BSA content was retained without the interferences from those in lower BSA samples. For samples with BSA >15%, the CEST contrast disappeared, presumably due to interactions between the compounds resulting in a reduction in exchange rate. We then applied NOMAR filtering to produce tissue-selective CEST contrast maps *in vivo*. Figs. 2A&2B show the T_2-w and NOMAR images for a mouse injected with Larg DLs, with the injected leg on the left of the image. A WASSR B_0 map is shown in Fig. 2C, with the variation in B_0 ~1000Hz (2.5 ppm). Figs. 2D and 2E show that, filtering by NOMAR < 0.7 produces a CEST map showing CEST contrast only within the lymph node by effectively separating 'hot spots' (yellow and blue arrowheads), which are likely induced by residual fat or fluid. This separation is verified by the mean MTR_{asym} plots of the selected ROI. This example clearly shows that tissue selection reduces the possibility of misinterpreted CEST signal due to erroneous tissues becoming cobtrast-enhanced, as facilitated by our NOMAR filter. The use of NOMAR is expected to be insensitive to small to moderate B_0 inhomogeneities (i.e. B_0 shifts < 1ppm) and B_1 inhomogeneities.

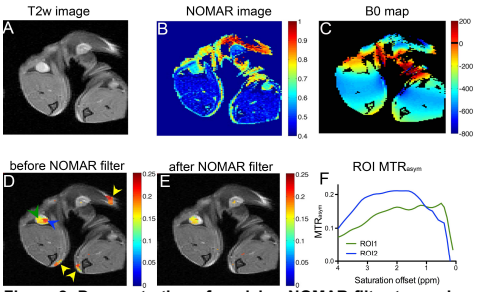

Figure 2. Demonstration of applying NOMAR filter to produce tissue-selective CEST contrast maps in lymphatic imaging using DLs. A) T2-w image; **B**) S (-12.5 ppm)/S(-50 ppm) map; **C**) WASSR B_0 map; **D**) and **E**) MTR_{asym} maps before and after NOMAR filtering, and **F**) MTR_{asym} plots of two ROIs as indicated by the green and blue arrows in **D**.

CONCLUSION

We proposed a new NOMAR segmentation technique for "cleaning up" CEST images. This can be accomplished by simply adding an acquisition of two additional saturation images to a CEST study.

REFERENCES (1)Ward, K. M.; Aletras, A. H.; Balaban, R. S. *J. Mag. Res.* **2000**, *143*, 79. (2)van Zijl, P. C.; Yadav, N. N. *Mag. Res. Med.* **2011**.(3)Guivel-Scharen, V.; Sinnwell, T.; Wolff, S. D.; Balaban, R. S. *J Mag. Res.* **1998**, *133*, 36.(4)Zhou, J.; Lal, B.; Wilson, D. A.; Laterra, J.; van Zijl, P. *Mag. Res. Med.* **2003**, *50*, 1120.(5)van Zijl, P. C.; Jones, C. K.; Ren, J.; Malloy, C. R.; Sherry, A. D. *PNAS* **2007**, *104*, 4359.(6)Henkelman, R.; Stanisz, G.; Graham, S. *NMR in Biomed.* **2001**, *14*, 57.(7)Stanisz, G. J.et. al. *Mag. Res. Med.* **2005**, *54*, 507.(8)Kalkers, N. F.; et al. *J Neurol Sci* **2001**, *184*, 155. (9)Parker, D. L.; et. Al. *Mag. Res. Med.* **1995**, *34*, 283. (10)Koenig, S. H.; Brown, R. D., 3rd; Ugolini, R. *Mag. Res. Med.* **1993**, *29*, 311. (11) Liu, G.; et al. **2011**. (12)Long, C. M.; van Laarhoven, H. W. M.; Bulte, J. W. M.; Levitsky, H. I. *Cancer Res.* **2009**, *69*, 3180. (13)Liu, G et al. *CMMI* **2010**, *5*, 162. ***Supported by NIH grants EB012590, EB015031, and EB015032.***